Published in final edited form as:
J Neuropathol Exp Neurol. 2010 September ; 69(9): 880–895. doi:10.1097/NEN.0b013e3181ed7a41.

Decreased Lin7b Expression in Layer 5 Pyramidal Neurons May Contribute to Impaired Corticostriatal Connectivity in Huntington Disease

Birgit Zucker, MD[1,3], **Jibrin A. Kama**[3], **Alexandre Kuhn, PhD**[2], **Doris Thu, PhD**[2], **Lianna R. Orlando, PhD**[3], **Anthone W. Dunah, PhD**[3], **Ozgun Gokce, PhD**[2], **David M. Taylor, PhD**[2], **Johann Lambeck, MD**[1], **Bernd Friedrich**[1], **Katrin S. Lindenberg, PhD**[4], **Richard L.M. Faull, MD, PhD**[5], **Cornelius Weiller, MD**[1], **Anne B. Young, MD, PhD**[3], and **Ruth Luthi-Carter, PhD**[2,3]

[1] Department of Neurology, University Hospital Freiburg, Germany [2]Brain Mind Institute, École Polytechnique Fédérale de Lausanne (EPFL), Lausanne, Switzerland [3]MassGeneral Institute for Neurodegenerative Disease (MIND), Department of Neurology, Massachusetts General Hospital and Harvard Medical School, Boston, Massachusetts [4]Department of Neurology, University of Ulm, Germany [5]Center for Brain Research and Department of Anatomy with Radiology, Faculty of Medical and Health Sciences, University of Auckland, New Zealand

Abstract

Motor dysfunction, cognitive impairment and regional cortical atrophy indicate cerebral cortical involvement in Huntington disease (HD). To address the hypothesis that abnormal corticostriatal connectivity arises from polyglutamine-related alterations in cortical gene expression, we isolated layer 5 cortical neurons by laser-capture microdissection and analyzed transcriptome-wide mRNA changes in them. Enrichment of transcription factor mRNAs including foxp2, tbr1, and neuroD6, and neurotransmission- and plasticity-related RNAs including sema5A, pclo, ntrk2, cntn1 and lin7b were observed. Layer 5 motor cortex neurons of transgenic R6/2 HD mice also demonstrated numerous transcriptomic changes, including decreased expression of mRNAs encoding the lin7 homolog b, (lin7b, also known as veli-2 and mals2). Decreases in LIN7B and CNTN1 RNAs were also detected in human HD layer 5 motor cortex neurons. lin7b, a scaffold protein implicated in synaptic plasticity, neurite outgrowth and cellular polarity, was decreased at the protein level in layer 5 cortical neurons in R6/2 mice and human HD brains. Decreases in Lin7b and Lin7a mRNAs were detected in R6/2 cortex as early as 6 weeks of age, suggesting that this is an early pathogenetic event. Thus, decreased cortical LIN7 expression may contribute to abnormal corticostriatal connectivity in HD.

Keywords

Corticostriatal projection; DNA microarray; huntingtin; LIN7; Polyglutamine disease; Striatum

Correspondence and reprint requests to: Prof. Ruth Luthi-Carter, Brain Mind Institute, Station 15, École Polytechnique Fédérale de Lausanne (EPFL), Lausanne, Switzerland. Tel. +41 21 693 9533; Fax. +41 21 693 9538. ruth.luthi-carter@epfl.ch.

INTRODUCTION

Huntington disease (HD) is an autosomal dominant polyglutamine disease characterized clinically by motor and cognitive dysfunction. The clinical features of HD have been attributed to neurodegeneration of subcortical basal ganglia circuits (1), but there is increasing evidence that the cerebral cortex may play a primary role in the pathobiology of HD. There are numerous structural and physiologic abnormalities in various cortical subregions, even in asymptomatic gene carriers (2). Transcranial magnetic stimulation, somatosensory evoked potentials and long latency reflexes show changes that suggest abnormal information processing and decreased excitability in motor and sensory cortices (3,4). Morphometric MRI studies also show that regionally selective thinning of the cortex occurs early in HD and correlates with cognitive impairment (5,6). At the cellular level, neuronal intranuclear inclusions (NIIs) indicate that mutant huntingtin protein (mt htt) accumulates in cortical projection neurons of layers 5 and 6 (7–9). We and others have shown that degeneration of pyramidal neurons in layers 3, 5 and 6 also occurs in HD (10,11). Interestingly, regionally selective layer 5 pyramidal neuron degeneration correlates with clinical heterogeneity in HD symptom profiles (12).

R6/2 mice express the N-terminal portion of human htt with ~150 CAG repeats, driven by the human *huntingtin* promoter (13). They exhibit severe learning and motor deficits, have NII from 3.5 weeks of age and have a limited lifespan of 12 to 17 weeks. Electrophysiological recordings of striatal medium spiny neurons from R6/2 animals reveal frequent large-amplitude synaptic events that indicate dysregulation of cortical inputs (14), which is consistent with the presumed corticostriatal dysfunction in HD. R6/2 mice also exhibit the striatal and cortical gene expression changes that occur in HD (15–17). Indeed, 12-week-old R6/2 mice bear greater striatal transcriptomic similarity to that of HD than any mt htt-expressing mice that have been studied to date (18).

We hypothesize that gene expression changes in corticostriatal projection neurons contribute to their dysfunction and that cortical mechanisms contribute to the selective neurodegeneration of striatal projection neurons due to disturbed connectivity. Therefore, we isolated layer 5 neurons of motor cortex (M1 and M2) from R6/2 and wild type (WT) mice by laser-capture microdissection (LCM) and compared their gene expression profiles using high-density microarrays. Layer 5 pyramidal cells were selected because the majority of corticostriatal projections originate from this layer (19,20), and because of the involvement of these cells in HD (10–12). To test the plausibility of this explanation for the selective striatal vulnerability characteristic of human HD, we subsequently assessed whether the changes observed in HD mice could also be detected in Brodmann areas 4 and 9 of human HD brain. To our knowledge, this is the first study to provide transcriptome-wide gene expression analyses of layer 5 neurons of the motor cortex and to assess the gene expression dysregulation in these cells in HD.

MATERIALS AND METHODS

Animals

Female R6/2 mice and WT littermates were purchased from Jackson Laboratories (Bar Harbor, ME) and killed at 12 weeks of age. Repeat length of the R6/2 mice used was approximately 141 to 152. Brains for LCM studies of R6/2 and WT littermates (4/group) were snap-frozen and stored at −80°C. Brains for homogenate studies were dissected from the skull and cortices of both hemispheres were immediately removed and snap-frozen.

RNA Samples and LCM

Eight-μm-thick sections from mouse brains and from human tissue blocks were cut on a cryostat (Shandon, Cheshire, UK) and thaw-mounted on uncoated glass slides (Gold Seal® RITE-ON micro slides, Thermo Fisher Scientific Inc., Rockford, IL). Sections were stained with methylene blue (Sigma, Steinheim, Germany), as previously described (21). Deep layer cortical neurons (mainly layer 5 but potentially including some layer 6) were selected from primary and secondary motor cortices (M1 and M2) of coronal mouse brain sections between +1.5 mm and +0.8 mm from Bregma (22). These lamina were defined in scanned images of each stained section by direct comparison to a mouse cytoarchitectonic atlas (22). Human deep layer cortical neurons were also selected by anatomical location in the lower third of the cortical ribbon in consultation with a neuropathologist Dr. M.P. Frosch (Massachusetts General Hospital, Boston, MA). Larger, triangular-shaped cell bodies of pyramidal cells were easily distinguishable from glia and interneurons on the basis of size and morphologic criteria (Fig. 1). Cells were selected using the PixCell II LCM instrument (Arcturus, Mountain View, CA), diameter 7.5 μm, onto CapSure™ HS caps covered with a thermoplastic film.

The harvested cells were solubilized from the film in extraction buffer provided in the Arcturus Pico Pure™ RNA isolation kit for 30 minutes at 42°C and stored at −80°C. The solubilized cells underwent RNA extraction according to the Pico Pure™ RNA isolation kit instructions (Arcturus), including a DNAse treatment step (Qiagen, Valencia, CA). Total murine cortex samples were homogenized and RNA was extracted using TRI reagent (Sigma) followed by RNeasy column clean up (Qiagen) using the manufacturers' protocols. RNA from both laser-dissected and homogenized samples was precipitated to achieve volume reduction.

Microarray Sample Processing

To establish conditions for the processing of total RNA isolated by LCM for microarray hybridization, we tested known concentrations of striatal homogenate RNA (1, 10, 50 ng) and LCM samples comprising 5000 striatal neurons of WT and R6/2 mouse brain in parallel following the GeneChip® Eukaryotic Small Sample Target Labeling Assay (Affymetrix, Santa Clara, CA, version 2). Analysis of the amplified samples on the Agilent Bioanalyzer (Agilent Technologies Inc., Santa Clara, CA) after the first round of amplifications showed typical cRNA size distributions (ranging between 400 and 2500 bp) and hybridization of second round cRNA showed the expected differential gene expression profiles (data not shown). 3'/5' ratios of Affymetrix control probe-sets revealed equivalent quality for 5 to 10 ng of homogenate and 5000 striatal neurons, although these ratios were systematically larger than for 1-cycle amplification. Because cortical pyramidal neurons are larger than striatal neurons (diameter 9–12 μm vs. 7.5–10 μm), we started with 4000 cortical neurons per animal, which we estimated to be equivalent to 5 ng of total RNA (21).

For layer 5 neurons, 20 ng of total RNA from each homogenized sample and RNA from 4000 laser-dissected neurons per sample were used to prepare biotinylated fragmented cRNA according to the GeneChip® Eukaryotic Small Sample Target Labeling Protocol with products from Affymetrix. Mouse Genome 430 2.0 Affymetrix GeneChip® Arrays were hybridized for 16 hours, washed, stained, and scanned using an Affymetrix Fluidics Station and Scanner (Biopolymers Facility, Harvard Medical School, Boston, MA).

Microarray Analysis

Selected array measures were reported from Affymetrix GCOS software; microarray data analyses were performed using R and Bioconductor packages (www.bioconductor.org). To compare gene expression in deep layer cortical neurons from R6/2 vs. WT animals, we

normalized 8 microarrays together (4 WT LCM and 4 R6/2 LCM) and quantified gene expression using robust multi-array analysis implemented in the R package affy (23–25). We identified differentially expressed genes in R6/2 LCM vs. WT LCM by computing empirical Bayes t-statistics with the R package limma (26). P values were corrected for multiple testing using the False Discovery Rate method (27). We used the same approach to assess gene enrichment in LCM vs. homogenate samples, normalizing and subsequently testing data from the 4 WT LCM vs. 4 WT homogenate microarrays. Microarray annotation was performed using the R package annotation tools (28) and Affymetrix annotation data.

Human Brain RNA Samples

Frozen blocks of motor cortex (BA4) and prefrontal association cortex (BA9) were obtained from Dr. J–P Vonsattel, New York Brain Bank, Columbia University, New York, NY. Pathological grading had been performed according to the Vonsattel scale (29) (Table 1). RNA quality was assessed by capillary electrophoresis with a Bioanalyzer 2100 (Agilent) using 500 ng of total RNA. RNA samples without sharp ribosomal RNA peaks were excluded from further processing steps; sample processing was performed as for mouse tissues.

Quantitative PCR Assays

Reverse transcription of RNA from human laser-dissected cortical neurons in BA4 and BA9 was conducted with a SuperScript™ First Strand Synthesis System for RT-PCR (Invitrogen, Carlsbad, CA), using random hexamer primers according to the manufacturer's instructions. Quantitative real-time PCR (q-PCR) assays were performed with a Bio-Rad iCycler (Hercules, CA) using SYBR-Green PCR Master Mix (Applied Biosystems, Foster City, CA) carrying out 50 PCR cycles as described (21). Each cDNA sample (equivalent to RNA from 50 laser-dissected neurons) was run in triplicate for the target and the normalizing gene in the same 96-well plate. Amplicon specificity was monitored by melt curve analysis at the end of the run, gel electrophoresis and DNA sequencing. Human primer sequences were as follows: LIN7B/MALS2 (**NM_022165**) CGCCCATCTACATCTCCC, AGCTCCACCGCCTTCTC; 28s rRNA (**M11167**) (30) AAACTCTGGTGGAGGTCCGT, CTTACCAAAAGTGGCCCACTA; CNTN1 (**NM_001843**) TGGCAAGCTGTATTCAACTCAC, GAGCCGCAGAAATTGGAAG; SYNCRIP (**NM_006372**) AGGTGCCCAACAACAAAGAG, CGCCGCTTGGAATCTG); ATP2B2 (**NM_001001331**) TCCTGGGCCATGCTGTCTAC, GGATCTTGCGGGCGTTG; VAMP1 (**NM_199245**) TGGGAACAGAGCGGAGAATG, TGGGAAACAAGGGCGAAAG, KCNK3 (**NM_002246**) GTGCTCATCGGCTTCTTCTC, TGCAGCGCCACGTAGTC; KCNA1 (**NM_000217**) AGATCGTGGGCTCCTTGTGT, AACTGCGGCGACTGAGGT; mGlUR2 (**NM_000839**) GGTGTTATTGGCGGTTCCTA, ATGTTGCGGGCACGA; GABRD (**NM_000815**) CCGAGACCTGCACAGATG, CCAGGCCAAGGCTTTATTTC; these were designed using Oligo 6.7 software (Molecular Biology Insights, Cascade, CO, USA). Primers for mouse Lin7 RNAs were as follows: Lin7a (NM_001039354) TTTCGAGAAGCTGCG GACA, TTCGAGCGCCTATGACATGTG); Lin7b (NM_011698) TAAGGCCACAGTGGCTGCTTT, CCCATGATGTTGAAGCCCAA; Lin7c (NM_011699) ATATCGCGGATAATTCCAGGTG, ATGGTG CTCCCCTTCAACACTC.

q-PCR Data Analysis

Expression of the mRNA of interest in each sample was calculated for q-PCR by normalization of C_t values to the reference RNA (28S rRNA) using the equation:

$$V=(1+E_{\text{reference}})^{(C_{t\ \text{reference}})}/(1+E_{\text{target}})^{(C_{t\ \text{target}})}$$

to correct for potential differences in PCR amplification efficiencies (21,31). V = relative value of target gene normalized to reference (28S rRNA), E = PCR amplification efficiency, C_t = threshold crossing cycle number. Differences between genotypes for human layer 5 cortical neurons were assessed using an unpaired, two-tailed Student *t*-test.

Immunoblotting

Sodium dodecyl sulfate polyacrylamide gel electrophoresis and transfer of separated proteins to PVDF membranes were performed as previously described (32). For protein electrophoresis, 15% polyacrylamide gels were employed. The concentration of lin7 antibody (Sigma) used for immunoblotting was 1 μg/ml. For quantification of lin7 protein, equal amounts (10 μg) of proteins from each group (6 R6/2 and 6 WT littermates) were loaded into each lane of the gel. Fyn kinase antibody was used as a loading control. Bands were visualized on film by enhanced chemiluminescence and their net intensities were quantified using computer-assisted densitometry (Kodak 1-D System, Rochester, NY). The net intensities of the bands were expressed as a percentage of that in control cortex and the resulting values were used to calculate group means. Differences between groups were analyzed using ANOVA with post hoc tests (Scheffe test). Statistical significance was taken to be $p < 0.05$.

Immunohistochemistry of Mouse Brain Sections

Six-μm-thick paraffin sagittal mouse brain sections from 4 R/2 and 4 WT littermates were run through xylene (Merck, Darmstadt, Germany) and a series of graded alcohols to phosphate buffered saline (PBS). Sections were then incubated in 10 mM Sodium Citrate pH 6.0 for 10 minutes, washed 3× 5 minutes in PBS, and incubated in 40% methanol and 1% H_2O_2 for 10 minutes to block endogenous peroxidase. Following washing (3× 10 minutes) in PBS, the sections were incubated in blocking solution (5% rabbit serum + 0.3 Triton X-100 in PBS) for 30 minutes at room temperature (RT), washed (3× 10 minutes) in PBS and then incubated overnight with the primary antibody (goat anti-lin7b; ab5967, Abcam, Cambridge, UK; 1:300) on a shaker at 4°C. The sections were then washed (3× 5 minutes) in PBS and incubated in a biotinylated anti-goat Ig (H+L) secondary antibody (Vector Laboratories Ltd., Peterborough, UK; 1:200) for 30 minutes at RT. Following additional washing (1× 5 minute, PBS), the sections were incubated in ABC reagent (metal enhanced DAB substrate kit, Thermo Fisher Scientific) for 30 minutes at RT and then exposed to DAB solution for 5 minutes. The sections were then washed in PBS, dried and dehydrated through a graded alcohol series to xylene and coverslipped with DPX mountant (Sigma Aldrich/Fluka, Steinheim, Germany).

Immunohistochemistry of Human Brain Sections

Tissues were obtained from the Neurological Foundation of New Zealand Human Brain Bank in the Center for Brain Research, University of Auckland. Fifty-μm-thick perfused-fixed, coronal sections of BA4 (motor cortex) were processed free-floating in 6-well tissue culture dishes. The sections were washed in PBS and 0.2% Triton-x (PBST), incubated for 20 minutes in 50% methanol and 1% H_2O_2, washed (3×10 minutes) in PBST; they were then incubated with the same goat anti-lin7b antibody as for mouse tissues (1:250) for 2 to 3 days on a shaker at 4°C. The sections were then washed (3×10 minutes, PBST) and incubated overnight in a biotinylated anti-goat Ig (H+L) secondary antibody (Vector, diluted 1:200). Following washing (3×10 minutes, PBST), the sections were incubated for 1 hour at RT in ABC mix, exposed to metal enhanced DAB (Thermo Fisher Scientific) for 5 minutes, and

then washed in PBST and mounted on gelatin-coated slides (Marienfeld Laboratory Glassware, Lauda-Koenigshofen, Germany; gelatin from Sigma), rinsed, dehydrated and coverslipped as above.

Image Analysis

Images of immunohistochemistry (IHC)-stained sections were collected and analyzed in a blinded fashion with respect to the sample genotype. For the human sections, a contour of the area of interest (layer V) in the primary motor cortex was first drawn at low power (4x) using Stereoinvestigator program (MicroBrightField, Williston, VT) using an Olympus BX60 microscope (Olympus Schweiz, Volketswil, Switzerland). Images were taken at 40x from the area within the defined boundary of each normal human and HD case. For mouse sections, images were taken at 20x from the striatum and the layer 5 of motor cortex. Images were analyzed using ImageJ (http://rsbweb.nih.gov/ij/) and Adobe Photoshop to measure the mean grey value. The difference between the normal and HD samples was assessed using a two-tailed Student *t*-test

RESULTS

RNAs Enriched in Layer 5 Cortical Neurons

To identify genes that exhibit enriched expression in layer 5 pyramidal neurons, we compared LCM and homogenate samples of mouse motor cortex (M1 and M2) in WT animals. 2943 (of 45037) array probe-sets reported increased expression by the relatively stringent False Discovery Rate criterion ($p < 0.05$) (Table 2; Supplementary Data Table 1). Several of these mRNAs or their corresponding proteins had been detected in cortical pyramidal neurons in previous studies. We detected the layer 5 enrichment of several transcription factors including: forkhead box P2 (foxp2) (33), T-box brain gene 1 (tbr1) (34), neurogenic differentiation 6 (neuroD6/nex-1) (35), FOG-2/Zfpm2 (36), and ets variants 3 and 5.

Selected synaptic and neurotransmission-related mRNAs were also enriched in layer 5 neurons, including vamp1 (vesicle associated membrane protein 1, also known as synaptobrevin), syncrip (synaptotagmin binding cytoplasmic RNA and interacting protein) (37,38), and pclo (piccolo) (39). Enrichment of mRNAs implicated in axon formation and targeting included contactin 1 (cntn1) (40), semaphorins (41) and eph receptors (42). Neurotrophic tyrosine kinase receptor type 2 (ntrk2, trkB) mRNA was also enriched in layer 5 cortical neurons compared to whole cortex, consistent with trkb protein localization in cortical axons, dendrites and glutamatergic synapses (43).

Dysregulated mRNA Expression in HD Mice

4732 (of 45037) array probe-sets indicated differential mRNA expression between deep layer cortical neurons from R6/2 vs. WT mice. Of the largest fold changes (1.75-fold or higher), 246 probe-sets detected decreases and 81 probe-sets detected increases in mRNA levels. Selected mRNAs showing differential expression in layer 5 R6/2 cortex are presented in Tables 3 and 4. Complete lists are in Supplementary Data Table 2.

Gene expression changes detected in the LCM array analysis included several mRNAs previously shown to be decreased in R6/2 cortex, including cplx2, dbp, sst, penk, arpp19, dusp1, and igfbp5 (16). The mRNA encoding igfbp4, which modulates the IGF/AKT prosurvival pathway (44), was also downregulated by more than 2-fold in R6/2 vs. WT layer 5 neurons. mRNAs encoding the $GABA_A$ receptor (GABRD) and Shaker-related member 1 of the voltage-gated potassium channel superfamily (kcna1) also showed 2-fold downregulation in R6/2 vs. control pyramidal cells (Table 3).

Some unanticipated changes in gene expression were also observed, including decreases in corticotropin releasing hormone (CRH) and its binding protein crhbp; this parallels a decrease in pituitary gland CRH levels in R6/2 mice (45). Other interesting changes revealed by this analysis included a decrease in the pyramidal cell enriched protease prss23 and several genes involved in immune system function (Tables 2–4). Intriguingly, there was upregulation of several mRNAs encoding transcriptional regulatory proteins previously linked to the biology of huntingtin (Table 4;Supplementary Data Table 2). These include the known huntingtin-interacting protein NCor1 (nuclear co-repressor 1) (46) and the repressor element 1 silencing transcription factor co-repressor 3 (RCoR3), a co-regulator of the NRSF/REST transcriptional silencing complex (47). mRNA expression of the ubiquitous co-repressor sin3b (which is known to be sequestered in polyglutamine aggregates) was also increased.

Pyramidal Cell-Enriched mRNAs Show Dysregulation in R6/2 Cortex

Previous studies indicate that a defect in neurotransmission could account for cognitive and motor deficits in HD. Accordingly, we determined whether mRNAs enriched in layer 5 pyramidal cells were dysregulated with polyglutamine disease in brains of R6/2 mice. Several layer 5-enriched synaptic proteins, including the SNARE complex synaptic vesicle protein vamp1, were downregulated. Brain-derived neurotrophic factor (BDNF), a cortically-expressed striatal neuron survival factor, showed a significant downregulation in HD layer 5 neurons but there was no significant enrichment in layer 5. Lin7b, a PDZ domain protein initially identified in *Caenorhabditis elegans* (48), was also decreased in corticostriatal neurons of R6/2 mice ($p < 0.0005$; Supplementary Data Table 2).

Similarities and Differences Between Transcriptomic Effects in Layer 5 R6/2 Neurons and Human BA4 HD Cortex

To assess whether cortical pyramidal mRNA changes in R6/2 mice might recapitulate mRNA changes in human motor cortex at a transcriptome-wide level, we compared LCM microarray profiles from R6/2 layer 5 cells to previously established microarray profiles of human BA4 cortex homogenates (17). Overlapping changes included decreased expression of mRNAs encoding neurotransmitter signaling pathway components (e.g. gad1, rgs4, itpr1), potassium channels (kcnc1, kcnc2), and other proteins involved in neurotransmission (e.g. vamp1, cplx2, arpp19, syt1) (Table 5; Supplementary Data Table 3). Interestingly, these comparisons also detected overlapping upregulation of mRNAs encoding neuronal signaling and viability regulators that were not reported in previous studies; these included increases in notch2 and Sirt1 (Table 5; Supplementary Data Table 3). Surprisingly, however, some of the above changes, including the apparent decreases in GABRD and plasma membrane ATPase Ca^{2+} transporting plasma membrane 2 (ATP2B2) RNAs, did not show a corresponding change in human HD layer 5 pyramidal cells by q-PCR (see below). This indicates that the decreases observed in HD BA4 cortex may occur in a different cell type such as pyramidal neurons of cortical layers 2/3 or GABAergic interneurons.

HD-Related Dysregulation of Gene Expression in Human Layer 5 Pyramidal Neurons

To determine to what extent the polyglutamine-induced mRNA changes in R6/2 pyramidal neurons might recapitulate the molecular changes that occur in the corresponding cell population in HD, we examined a subset of these changes in human HD cases and controls using q-PCR on layer 5 cortical neurons from both Brodmann area 4 (primary motor cortex) and Brodmann area 9 (prefrontal association cortex) for each HD case or control (Table 1). Because HD brain revealed a downregulation of β-actin, the ribosomal 28s RNA was used for normalization.

Because layer 5 neurons degenerate selectively in HD cortex, we assessed genes enriched in layer 5 pyramidal cells. A similar hypothesis has been proposed for the selective degeneration medium spiny neurons in the HD striatum (49,50). However, in contrast to findings in striatum, only a very small proportion of the tested layer 5-enriched genes were significantly downregulated in human HD pyramidal cells. mRNAs with normal expression levels in HD layer 5 neurons included VAMP1, SYNCRIP, voltage gated potassium channel subfamily members KCNA1 (control 60.1 ± 8.6, HD 42.5 ± 9.9, $p > 0.1$) and KCNK3 (control 3.9 ± 1.3, HD 2.5 ± 1.3, $p > 0.5$), ATP2B2 and metabotropic glutamate receptor 2 (control 2.8 ± 0.95, HD: 3.1 ± 1.1, $p>0.5$). On the other hand, the RNA encoding CNTN1 was significantly decreased in human HD BA4 pyramidal cells (Fig. 2).

We next determined whether differential expression in R6/2 layer 5 motor neurons predicted corresponding layer 5 changes in human HD cortex. Although RNAs encoding voltage-gated potassium channels or GABRD subunit were not significantly diminished in either BA4 (control 0.004 ± 0.001, HD 0.002 ± 0.0007, $p > 0.2$) or BA9 samples, the RNA encoding lin7b was significantly decreased in BA4 and showed a non-significant trend toward decrease in BA9 (Fig. 2). The selective decrease in the expression of this neuronal connectivity-related molecule in human HD cortex motivated us to verify a change in lin7 at the protein level and consider is possible functional consequences.

Lin7b Protein Levels

R6/2 cortical protein lysates were analyzed by Western blot with a pan-lin7 antibody. As shown in Figure 3A, we observed 2 bands of corresponding to apparent molecular weights of 21–27 kDa representing lin7 isoforms lin7a, b and c / mals1, 2 and 3, consistent with previous observations (51). Comparison of the abundance of lin7+ species in R6/2 cortex with control revealed significant decreases in both lin7+ bands (Fig. 3A, B). To investigate these changes, we also performed IHC analyses of LIN7B protein using a lin7b-specific antibody. We found that LIN7B was significantly decreased in layer 5 pyramidal cortical neurons in both R6/2 mice and in human HD brains (Figs. 4A, B, 5). Thus, lin7b RNA levels are paralleled by decreases in lin7b protein in cortical projection cells.

To assess whether lin7b expression would also be decreased in cortical axons in the striatum, we performed additional IHC on R6/2 mice. Quantification of lin7b immunoreactivity in axon fiber-containing striatal white matter tracts also showed decreased lin7b expression (Fig. 4C, D). Although it is unlikely that all such fibers terminate in the striatum, these results indicate that a parallel diminution of expression occurs in axonal as well as cell body compartments of cortical projection neurons. To determine whether decreased Lin7b expression may contribute to HD-related dysfunction early in the disease process, we measured cortical RNA levels in younger R6/2 mice by q-PCR. Lin7b RNA was significantly decreased by 6 weeks of age, coincident with the onset of early motor deficits in these mice (52). Lin7b RNA was also significantly decreased at 8 and 10 weeks of age. Consistent with the Western blots in 12-week-old animals (Fig. 3), Lin7a RNA was also decreased significantly at 6, 8, and 10 weeks of age (Fig. 6). Thus, the early and persistent decreases in Lin7a and Lin7b expression are consistent with a role in HD etiology. In contrast, Lin7c RNA showed only a transient increase at 8 weeks, which would be more consistent with a compensatory effect than an etiologic role in HD (Fig. 6).

DISCUSSION

Diminished expression of LIN7A and LIN7B mRNAs and proteins in HD cortex provides novel evidence for a role of LIN7 in the pathogenesis of HD. In view of its known role in neuronal connectivity, we conclude that an HD-associated decrease in LIN7 expression in cortical projection neurons is a plausible mechanism of corticostriatal dysfunction.

Cortical Pyramidal Cells and HD

Abnormal connectivity between the cortex and the basal ganglia may account for cognitive and/or motor manifestations of HD. Dysfunction of corticostriatal projections has been considered in previous studies of R6/2 mice as electrophysiological recordings reveal decreased EPSCs in striatal medium spiny neurons and large-amplitude synaptic events that indicate dysregulation of cortical glutamatergic inputs (14). NMDA receptor currents of cortical pyramidal neurons from R6/2 mice become smaller than those of WT mice beginning at 21 days of age (53). Here, we addressed the possibility that transcriptional alterations contribute to the HD-related dysfunction of corticostriatal projection neurons.

To avoid the confounding effects of cellular heterogeneity and the potential for changes in cell ratios during the neurodegenerative process, we performed a targeted cellular expression analysis using LCM. Because most of the projections to the striatum originate from layer 5 (19,20), we collected medium- and large-sized pyramidal cells of this lamina. Pyramidal neurons within layer 5 form 2 subtypes: type 1 pyramidal neurons projecting to the superior colliculus, spinal cord, basal pons and striatum and type 2 projecting to the contralateral cortex and ipsilateral striatum (20,54). Both project to the striatum and we did not differentiate between these 2 subtypes; presumably both were sampled in their endogenous proportions. Since layer 6 cortical neurons cannot easily be distinguished from layer 5 neurons, it is also possible that some layer 6 cells were included in our samples; this should be inconsequential to the interpretation of the data, because layer 6 neurons also project to the striatum.

The decreased $GABA_A$ receptor delta subunit expression observed in R6/2 layer 5 neurons (Table 3) and in human HD cortex homogenates (17) suggests that neocortical GABAergic signaling (55,56) might be altered in HD, which would comprise an interesting area of future investigation. However, based on the human LCM data, additional data are required to attribute this change to a specific neuronal population in the human HD brain.

Some RNA changes observed in R6/2 layer 5 cells did not show corresponding changes in human BA4 or BA9. Possible explanations for this are that these changes do not occur to the same extent in the HD brain, or that they occur in a limited subset of cells that escaped detection in the current study. These changes may alternatively indicate possible mt htt effects in other cortical neurons, such as layer 3 pyramidal cells, other layer 5 pyramidal cells, or GABAergic interneurons. Indeed, comparisons with our previous microarray analyses of human HD brain also infer that transcriptomic perturbations occur in cortical cells other than layer 5 pyramidal neurons. For example, whereas human BA4 tissue homogenates show significant decreases in GABRD and ATP2B2 mRNAs, the present experiments demonstrate that layer 5 pyramidal neurons in BA4 do not harbor these changes. Thus, additional anatomical and molecular studies to clarify transcriptional perturbations in other cortical cell types are warranted

HD-Related Transcriptional Dysregulation in Corticostriatal Neurons

Changes in gene expression shared by R6/2 layer 5 pyramidal cells and human HD BA4 likely represent early, relevant molecular events in HD pathogenesis. The distribution of mRNA changes (i.e. 3 times more decreases than increases) is in accordance with previous microarray results from other neurons of R6/2 mice and from LCM samples of human HD grade 1 brains (17,49).

Using LCM, we were able to identify cortical mRNAs that show enriched expression in layer 5 pyramidal neurons (Table 2). As expected, the expression of most layer 5 enriched genes did not change in HD-affected neurons; however, CNTN 1 was both enriched in layer 5 and downregulated in human corticostriatal cells (Fig. 2). Contactin 1, an axonal

glycoprotein belonging to the immunoglobulin family of cell adhesion molecules, was enriched in layer 5 cortical neurons, which is in line with data from an in situ hybridization histochemical study that showed expression of this molecule in layers 2, 3 and 5. It is thought to play an important role in axonal pathfinding in development and its plasma membrane signal transduction activity has been shown to govern the formation and maintenance of synapses (40,57). Therefore, we postulate that downregulation of CNTN1 in human HD BA4 cortex (to 44.4 % of control levels) could contribute to the destabilization of corticostriatal connections.

Although there are biochemical data to suggest that the general transcriptional machinery is affected by mutant huntingtin, the discrete subpopulations of neuronal RNAs affected in model systems suggests a more specific mechanism or set of mechanisms. We observed aberrant expression of RNAs encoding known huntingtin-interacting transcriptional regulators. Specifically, NCoR1, and REST corepressor 3 are upregulated in R6/2 cortical neurons, as well as sin3b, another co-regulator that can be present in either NCoR or REST complexes. Whereas increased transcriptional repression by these factors has been previously attributed to direct interactions with mt htt (58), our data raise the possibility that increased expression levels of these factors contribute to a change in their activities. However, the extent to which these expression changes have functional relevance to primary or secondary disease events remains to be determined.

Regional Differences in Human HD Cortex

To assess the potential impacts of gene expression changes on both motor and cognitive dysfunction, we examined both BA4 (primary motor cortex) and BA9 (prefrontal association cortex). As expected, cortical neurons from BA4 revealed transcriptomic dysregulation whereas layer 5 neurons from BA9 showed no significant changes in gene expression, although there was a trend towards downregulation for some mRNAs (Fig. 2). This is in accordance with a parallel microarray analysis of HD brain in which BA4 but not BA9 exhibited significant changes in mRNA levels (17). It is also in agreement with the findings functional MRI-based volumetric regional thinning in BA4 of HD gene carriers (5).

Decreased Levels of lin7b as a New Potential Mechanism of Corticostriatal Dysfunction in HD

Neurons are highly polarized cells with intricate functional specifications of presynaptic axons and postsynaptic dendrites (59); specialized polarity proteins participate in axon formation, growth and synaptogenesis, in part through signaling to the actin and microtubule cytoskeletons. The 3 members of the mammalian lin7 family of proteins comprise PDZ domain-containing scaffolding proteins that have also been previously shown to couple cell adhesion to intercellular signaling (51,60). Mice harboring null mutations of all 3 lin7 isoforms die perinatally with respiratory problems and deficient synaptic transmission (61). Our data reveal enrichment of lin7b in layer 5 pyramidal neurons and show that it is downregulated in both R6/2 mice and in human HD layer 5 neurons. Based on the R6/2 mouse results, it also seems possible that Lin7a expression may be decreased in HD brain. Reduced levels of either Lin7b or Lin7a might disrupt normal neuronal connectivity and/or plasticity, either within the cerebral cortex or between the cortex and the basal ganglia. Therefore we hypothesize that decreased Lin7 levels contribute to functional deficits in HD brain an issue warranting further assessment in future studies.

The present data add to the growing body of molecular and functional evidence that corticostriatal communication is abnormal in the HD brain. A recent electrophysiological study also revealed progressive derailment of long-term depression and short term plasticity of corticostriatal neurons at perirhinal synapses in HD mice (62). Likewise, Golgi stains of

human HD brain sections reveal marked recurving of dendritic branches in striatal medium spiny neurons together with altered dendritic spine density, consistent with decreased structural or signaling plasticity (63). Still other recent evidence for deficits of BDNF synthesis and transport along the corticostriatal axons (64) provides an additional candidate mechanism underlying decreased corticostriatal connectivity. Thus, further investigation is warranted to determine to what extent the loss of lin7b, lin7a, or contactin 1 or other etiologic events might account for decreased communication between the cortex and the basal ganglia in HD.

Supplementary Material

Refer to Web version on PubMed Central for supplementary material.

Acknowledgments

The authors wish to thank Dr. Jean Paul Vonsattel and the New York Brain Bank, Taub Institute, Columbia University (NYBB), New York, for providing the postmortem human brains, Dr. Sarah J. Augood for helpful advice on laser capture microdissection and Dr. Matthew P. Frosch for consultation on neuroanatomical and neurocytologic aspects of the study. We also thank Dr. Ippolita Cantuti Castelvetri, Dr. Sandra Dieni and Markus Kelm for valuable discussions and technical support.

This study was supported by the Hereditary Disease Foundation, the EPFL, the National Institutes of Health (Grant NS045242 to R.L.-C. and AG13617 to A.B.Y.), and the Deutsche Forschungsgemeinschaft grant ZU125/1-1 (to B.Z.) and the Neurological Foundation of New Zealand and the Health Research Council of New Zealand.

REFERENCES

1. Vonsattel JP, DiFiglia M. Huntington disease. J Neuropathol Exp Neurol. 1998; 57:369–384. [PubMed: 9596408]
2. Kloppel S, Draganski B, Siebner HR, et al. Functional compensation of motor function in pre-symptomatic Huntington's disease. Brain. 2009; 132:1624–1632. [PubMed: 19369489]
3. Berardelli A, Noth J, Thompson PD, et al. Pathophysiology of chorea and bradykinesia in Huntington's disease. Mov Disord. 1999; 14:398–403. [PubMed: 10348461]
4. Lorenzano C, Dinapoli L, Gilio F, et al. Motor cortical excitability studied with repetitive transcranial magnetic stimulation in patients with Huntington's disease. Clin Neurophysiol. 2006; 117:1677–1681. [PubMed: 16793338]
5. Rosas HD, Hevelone ND, Zaleta AK, et al. Regional cortical thinning in preclinical Huntington disease and its relationship to cognition. Neurology. 2005; 65:745–747. [PubMed: 16157910]
6. Rosas HD, Liu AK, Hersch S, et al. Regional and progressive thinning of the cortical ribbon in Huntington's disease. Neurology. 2002; 58:695–701. [PubMed: 11889230]
7. DiFiglia M, Sapp E, Chase KO, et al. Aggregation of huntingtin in neuronal intranuclear inclusions and dystrophic neurites in brain. Science. 1997; 277:1990–1993. [PubMed: 9302293]
8. Sapp E, Penney J, Young A, et al. Axonal transport of N-terminal huntingtin suggests early pathology of corticostriatal projections in Huntington disease. J Neuropathol Exp Neurol. 1999; 58:165–173. [PubMed: 10029099]
9. Sieradzan KA, Mann DM. The selective vulnerability of nerve cells in Huntington's disease. Neuropathol Appl Neurobiol. 2001; 27:1–21. [PubMed: 11298997]
10. Sotrel A, Paskevich PA, Kiely DK, et al. Morphometric analysis of the prefrontal cortex in Huntington's disease. Neurology. 1991; 41:1117–1123. [PubMed: 1829794]
11. Macdonald V, Halliday G. Pyramidal cell loss in motor cortices in Huntington's disease. Neurobiol Dis. 2002; 10:378–386. [PubMed: 12270698]
12. Thu DC, Oorschot DE, Tippett LJ, et al. Cell loss in the motor and cingulate cortex correlates with symptomatology in Huntington's disease. Brain. 2010; 133:1094–1110. [PubMed: 20375136]

13. Mangiarini L, Sathasivam K, Seller M, et al. Exon 1 of the HD gene with an expanded CAG repeat is sufficient to cause a progressive neurological phenotype in transgenic mice. Cell. 1996; 87:493–506. [PubMed: 8898202]

14. Cepeda C, Hurst RS, Calvert CR, et al. Transient and progressive electrophysiological alterations in the corticostriatal pathway in a mouse model of Huntington's disease. J Neurosci. 2003; 23:961–969. [PubMed: 12574425]

15. Augood SJ, Faull RL, Love DR, et al. Reduction in enkephalin and substance P messenger RNA in the striatum of early grade Huntington's disease: A detailed cellular in situ hybridization study. Neuroscience. 1996; 72:1023–1036. [PubMed: 8735227]

16. Luthi-Carter R, Hanson SA, Strand AD, et al. Dysregulation of gene expression in the R6/2 model of polyglutamine disease: Parallel changes in muscle and brain. Hum Mol Genet. 2002; 11:1911–1926. [PubMed: 12165554]

17. Hodges A, Strand AD, Aragaki AK, et al. Regional and cellular gene expression changes in human Huntington's disease brain. Hum Mol Genet. 2006; 15:965–977. [PubMed: 16467349]

18. Kuhn A, Goldstein DR, Hodges A, et al. Mutant huntingtin's effects on striatal gene expression in mice recapitulate changes observed in human Huntington's disease brain and do not differ with mutant huntingtin length or wild-type huntingtin dosage. Hum Mol Genet. 2007; 16:1845–1861. [PubMed: 17519223]

19. McGeorge AJ, Faull RL. The organization of the projection from the cerebral cortex to the striatum in the rat. Neuroscience. 1989; 29:503–537. [PubMed: 2472578]

20. Reiner A, Jiao Y, Del Mar N, et al. Differential morphology of pyramidal tract-type and intratelencephalically projecting-type corticostriatal neurons and their intrastriatal terminals in rats. J Comp Neurol. 2003; 457:420–440. [PubMed: 12561080]

21. Zucker B, Luthi-Carter R, Kama JA, et al. Transcriptional dysregulation in striatal projection- and interneurons in a mouse model of Huntington's disease: Neuronal selectivity and potential neuroprotective role of HAP1. Hum Mol Genet. 2005; 14:179–189. [PubMed: 15548548]

22. Hof PR, Young WG, Bloom FE, Belichenko PV, Celio MR. Comparative Cytoarchitectonic Atlas of the C57BL/6 and 129/Sv Mouse Brains. 2000

23. Bolstad BM, Irizarry RA, Astrand M, et al. A comparison of normalization methods for high density oligonucleotide array data based on variance and bias. Bioinformatics. 2003; 19:185–193. [PubMed: 12538238]

24. Irizarry RA, Bolstad BM, Collin F, et al. Summaries of Affymetrix GeneChip probe level data. Nucleic Acids Res. 2003; 31:e15. [PubMed: 12582260]

25. Gautier L, Cope L, Bolstad BM, et al. affy--analysis of Affymetrix GeneChip data at the probe level. Bioinformatics. 2004; 20:307–315. [PubMed: 14960456]

26. Smyth GK. Linear models and empirical bayes methods for assessing differential expression in microarray experiments. Stat Appl Genet Mol Biol. 2004; 3 Article 3.

27. Benjamini H. Controlling the false discovery rate: A practical and powerful approach to multiple testing. J Royal Stat Soc. 1995; 57:289–300. series B.

28. Kuhn A, Luthi-Carter R, Delorenzi M. Cross-species and cross-platform gene expression studies with the Bioconductor-compliant R package 'annotationTools'. BMC Bioinformatics. 2008; 9:26. [PubMed: 18201381]

29. Vonsattel JP, Myers RH, Stevens TJ, et al. Neuropathological classification of Huntington's disease. J Neuropathol Exp Neurol. 1985; 44:559–577. [PubMed: 2932539]

30. Naito E, Dewa K, Ymanouchi H, et al. Ribosomal ribonucleic acid (rRNA) gene typing for species identification. J Forensic Sci. 1992; 37:396–403. [PubMed: 1500890]

31. Ferrante RJ, Kubilus JK, Lee J, et al. Histone deacetylase inhibition by sodium butyrate chemotherapy ameliorates the neurodegenerative phenotype in Huntington's disease mice. J Neurosci. 2003; 23:9418–9427. [PubMed: 14561870]

32. Dunah AW, Yasuda RP, Wang YH, et al. Regional and ontogenic expression of the NMDA receptor subunit NR2D protein in rat brain using a subunit-specific antibody. J Neurochem. 1996; 67:2335–2345. [PubMed: 8931465]

33. White SA, Fisher SE, Geschwind DH, et al. Singing mice, songbirds, and more: models for FOXP2 function and dysfunction in human speech and language. J Neurosci. 2006; 26:10376–10379. [PubMed: 17035521]
34. Bulfone A, Smiga SM, Shimamura K, et al. T-brain-1: A homolog of Brachyury whose expression defines molecularly distinct domains within the cerebral cortex. Neuron. 1995; 15:63–78. [PubMed: 7619531]
35. Bartholoma A, Nave KA. NEX-1: A novel brain-specific helix-loop-helix protein with autoregulation and sustained expression in mature cortical neurons. Mech Dev. 1994; 48:217–228. [PubMed: 7545978]
36. Holmes M, Turner J, Fox A, et al. hFOG-2, a novel zinc finger protein, binds the co-repressor mCtBP2 and modulates GATA-mediated activation. J Biol Chem. 1999; 274:23491–23498. [PubMed: 10438528]
37. Mochida S. Protein-protein interactions in neurotransmitter release. Neurosci Res. 2000; 36:175–182. [PubMed: 10683521]
38. Mizutani A, Fukuda M, Ibata K, et al. SYNCRIP, a cytoplasmic counterpart of heterogeneous nuclear ribonucleoprotein R, interacts with ubiquitous synaptotagmin isoforms. J Biol Chem. 2000; 275:9823–9831. [PubMed: 10734137]
39. Fejtova A, Gundelfinger ED. Molecular organization and assembly of the presynaptic active zone of neurotransmitter release. Results Probl Cell Differ. 2006; 43:49–68. [PubMed: 17068967]
40. Virgintino D, Ambrosini M, D'Errico P, et al. Regional distribution and cell type-specific expression of the mouse F3 axonal glycoprotein: A developmental study. J Comp Neurol. 1999; 413:357–372. [PubMed: 10502245]
41. Polleux F, Morrow T, Ghosh A. Semaphorin 3A is a chemoattractant for cortical apical dendrites. Nature. 2000; 404:567–573. [PubMed: 10766232]
42. Mann F, Peuckert C, Dehner F, et al. Ephrins regulate the formation of terminal axonal arbors during the development of thalamocortical projections. Development. 2002; 129:3945–3955. [PubMed: 12135931]
43. Gomes RA, Hampton C, El-Sabeawy F, et al. The dynamic distribution of TrkB receptors before, during, and after synapse formation between cortical neurons. J Neurosci. 2006; 26:11487–11500. [PubMed: 17079678]
44. Durai R, Davies M, Yang W, et al. Biology of insulin-like growth factor binding protein-4 and its role in cancer (review). Int J Oncol. 2006; 28:1317–1325. [PubMed: 16685432]
45. Bjorkqvist M, Petersen A, Bacos K, et al. Progressive alterations in the hypothalamic-pituitary-adrenal axis in the R6/2 transgenic mouse model of Huntington's disease. Hum Mol Genet. 2006; 15:1713–1721. [PubMed: 16613897]
46. Boutell JM, Thomas P, Neal JW, et al. Aberrant interactions of transcriptional repressor proteins with the Huntington's disease gene product, huntingtin. Hum Mol Genet. 1999; 8:1647–1655. [PubMed: 10441327]
47. Zuccato C, Tartari M, Crotti A, et al. Huntingtin interacts with REST/NRSF to modulate the transcription of NRSE-controlled neuronal genes. Nat Genet. 2003; 35:76–83. [PubMed: 12881722]
48. Ferguson EL, Horvitz HR. Identification and characterization of 22 genes that affect the vulval cell lineages of the nematode Caenorhabditis elegans. Genetics. 1985; 110:17–72. [PubMed: 3996896]
49. Luthi-Carter R, Strand A, Peters NL, et al. Decreased expression of striatal signaling genes in a mouse model of Huntington's disease. Hum Mol Genet. 2000; 9:1259–1271. [PubMed: 10814708]
50. Desplats PA, Kass KE, Gilmartin T, et al. Selective deficits in the expression of striatal-enriched mRNAs in Huntington's disease. J Neurochem. 2006; 96:743–757. [PubMed: 16405510]
51. Jo K, Derin R, Li M, et al. Characterization of MALS/Velis-1, −2, and −3: A family of mammalian LIN-7 homologs enriched at brain synapses in association with the postsynaptic density-95/NMDA receptor postsynaptic complex. J Neurosci. 1999; 19:4189–4199. [PubMed: 10341223]
52. Carter RJ, Lione LA, Humby T, et al. Characterization of progressive motor deficits in mice transgenic for the human Huntington's disease mutation. J Neurosci. 1999; 19:3248–3257. [PubMed: 10191337]

53. Andre VM, Cepeda C, Venegas A, et al. Altered cortical glutamate receptor function in the R6/2 model of Huntington's disease. J Neurophysiol. 2006; 95:2108–2119. [PubMed: 16381805]
54. Molnar Z, Cheung AF. Towards the classification of subpopulations of layer V pyramidal projection neurons. Neurosci Res. 2006; 55:105–115. [PubMed: 16542744]
55. Vruwink M, Schmidt HH, Weinberg RJ, et al. Substance P and nitric oxide signaling in cerebral cortex: Anatomical evidence for reciprocal signaling between two classes of interneurons. J Comp Neurol. 2001; 441:288–301. [PubMed: 11745651]
56. Bacci A, Rudolph U, Huguenard JR, et al. Major differences in inhibitory synaptic transmission onto two neocortical interneuron subclasses. J Neurosci. 2003; 23:9664–9674. [PubMed: 14573546]
57. Falk J, Bonnon C, Girault JA, et al. F3/contactin, a neuronal cell adhesion molecule implicated in axogenesis and myelination. Biol Cell. 2002; 94:327–334. [PubMed: 12500940]
58. Zuccato C, Belyaev N, Conforti P, et al. Widespread disruption of repressor element-1 silencing transcription factor/neuron-restrictive silencer factor occupancy at its target genes in Huntington's disease. J Neurosci. 2007; 27:6972–6983. [PubMed: 17596446]
59. Wiggin GR, Fawcett JP, Pawson T. Polarity proteins in axon specification and synaptogenesis. Dev Cell. 2005; 8:803–816. [PubMed: 15935771]
60. Butz S, Okamoto M, Sudhof TC. A tripartite protein complex with the potential to couple synaptic vesicle exocytosis to cell adhesion in brain. Cell. 1998; 94:773–782. [PubMed: 9753324]
61. Olsen O, Moore KA, Fukata M, et al. Neurotransmitter release regulated by a MALS-liprin-alpha presynaptic complex. J Cell Biol. 2005; 170:1127–1134. [PubMed: 16186258]
62. Cummings DM, Milnerwood AJ, Dallerac GM, et al. Aberrant cortical synaptic plasticity and dopaminergic dysfunction in a mouse model of huntington's disease. Hum Mol Genet. 2006; 15:2856–2868. [PubMed: 16905556]
63. Graveland GA, Williams RS, DiFiglia M. Evidence for degenerative and regenerative changes in neostriatal spiny neurons in Huntington's disease. Science. 1985; 227:770–773. [PubMed: 3155875]
64. Gauthier LR, Charrin BC, Borrell-Pages M, et al. Huntingtin controls neurotrophic support and survival of neurons by enhancing BDNF vesicular transport along microtubules. Cell. 2004; 118:127–138. [PubMed: 15242649]

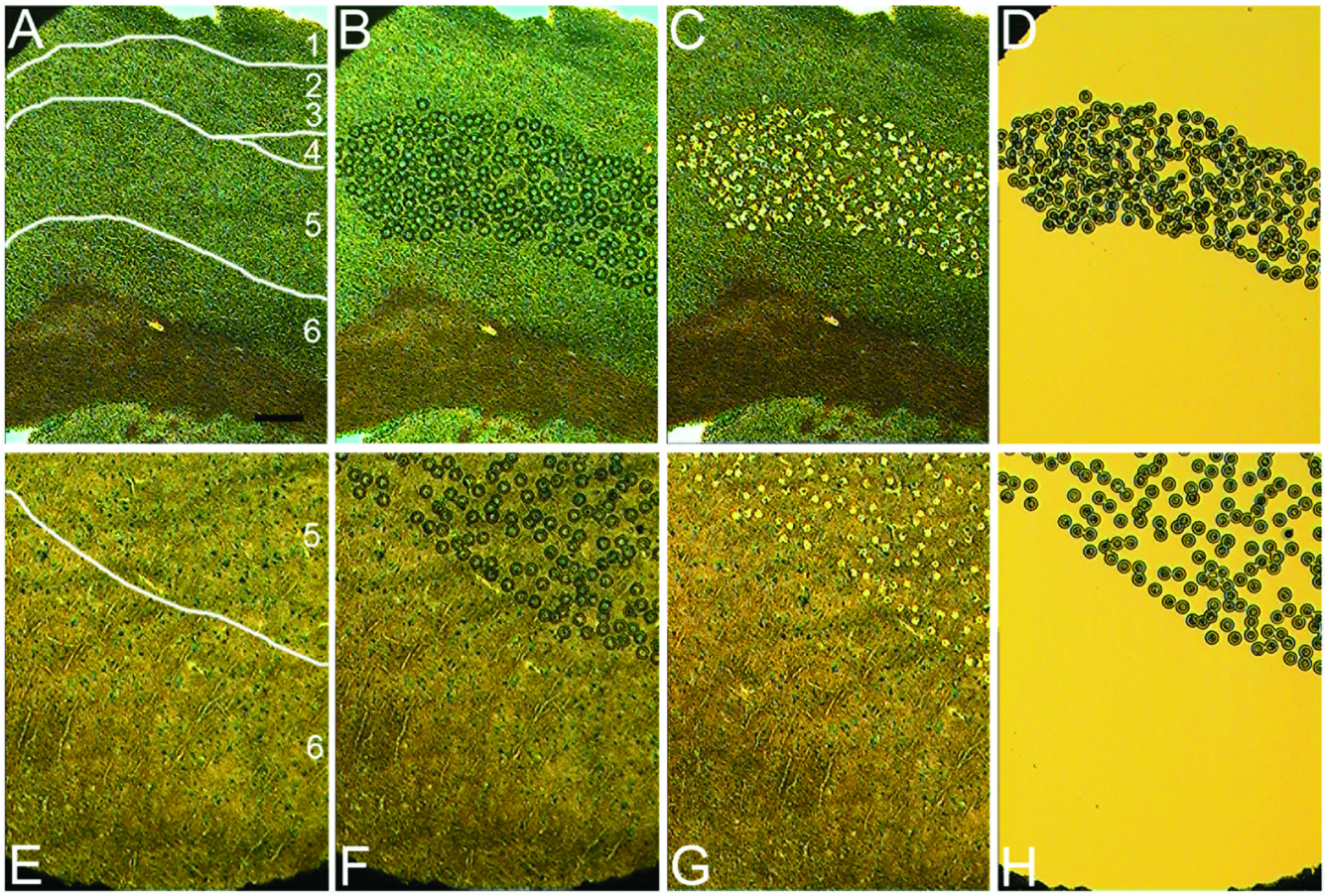

Figure 1.

Visualization of murine and human deep layer cortical neurons for laser capture microdissection (LCM). (**A–D**) Sections from cortex of 12-week-old R6/2 mice show the 6 cortical layers (**A**), neurons chosen for dissection (**B**), the section after LCM (**C**) and the harvested neurons attached to a thermoplastic film (**D**). (**E–H**) Cortex from grade 2 Huntington disease show a layer 5,6 in a coronal section (**E**), layer 5 neurons selected for LCM (**F**), the section after LCM (**G**) and harvested cortical perikarya (**H**). All are stained with methylene blue. Bar = 250 μm.

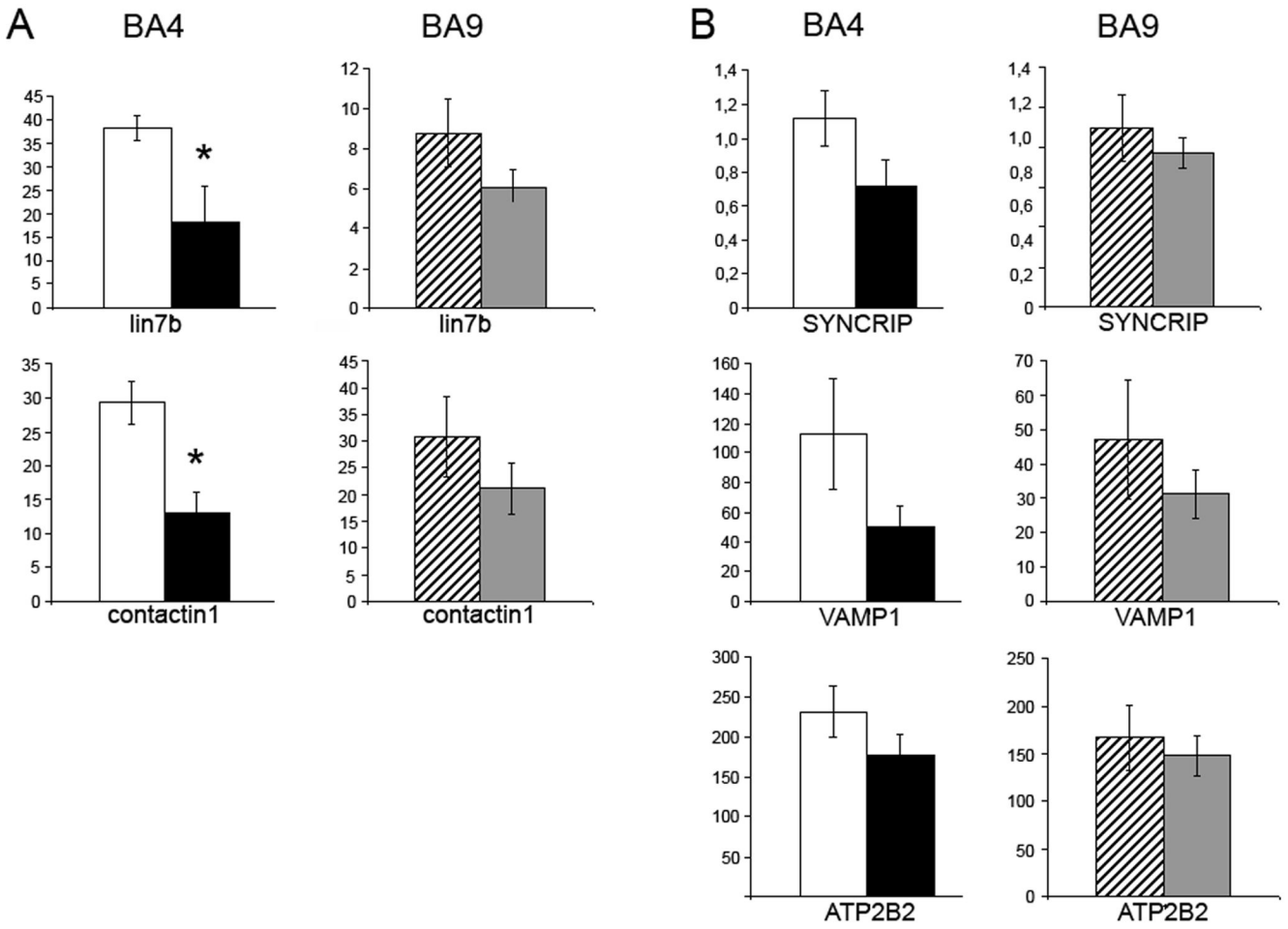

Figure 2.

Quantitative PCR analysis of mRNA expression levels in layer 5 cortical neurons in Huntington disease (HD) (n = 9) vs. control (n = 8) samples. Bar graphs show relative expression measures (i.e. number × 10^{-6}) normalized to 28S rRNA. White bar: control cortex BA4, black bar: HD cortex BA4, diagonally striped bar: control cortex BA9, dark grey bar: HD cortex BA9. Each sample was run in triplicate. Error bars = SEM; *$p < 0.05$: n.s. = not significant. (**A**) lin7b was decreased to 47.8% in HD BA4 vs. control BA4 ($p < 0.01$). lin7b did not differ between HD and control BA9 (n.s.). Contactin 1 mRNA in deep layer cortical neurons of BA 4 was decreased to 44.4% in HD vs. control ($p < 0.02$); there is no difference in BA9 (n.s.). (**B**) mRNA expression that is not significantly changed in human HD cortical layer 5 neurons. SYNCRIP shows a trend to a decrease in HD cortex that is not significant in either BA4 ($p > 0.05$) or BA9 ($p > 0.5$). VAMP1 does not show an HD-related change in either region ($p > 0.2$; $p > 0.5$). ATP2B2 also is not significantly different between HD and control ($p > 0.1$; $p > 0.2$). Additional mRNAs were assayed in BA4 layer 5 neurons but did not show an appreciable difference in HD versus controls (not shown).

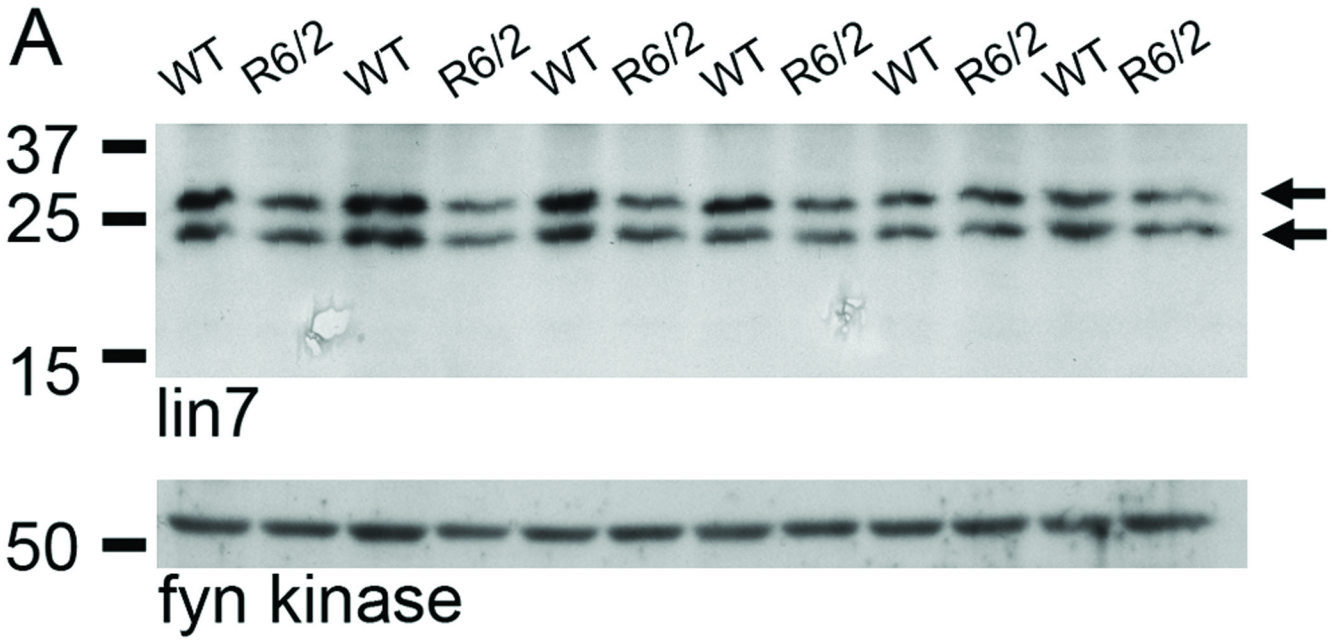

Figure 3.

lin7 protein is decreased in R6/2 transgenic mice. (**A**) Cortical homogenates from wild type (WT) and R6/2 mice were analyzed by Western blot with a pan-lin7 antibody and a Fyn kinase antibody as a loading control. There are 2 bands of immunoreactivity corresponding to apparent molecular weights of 21–27 kDa. (**B**) Densitometric analysis of lin7 protein levels from the blot shown in **A**, expressed as mean ± SEM percent abundance in R6/2 and control (100%) mice. Light grey and dark grey bars, WT; black and diagonally striped bars, R6/2. Error bars = SEM. The values for both bands in R6/2 mice are significantly different from the WT ($p < 0.05$; $n = 6$).

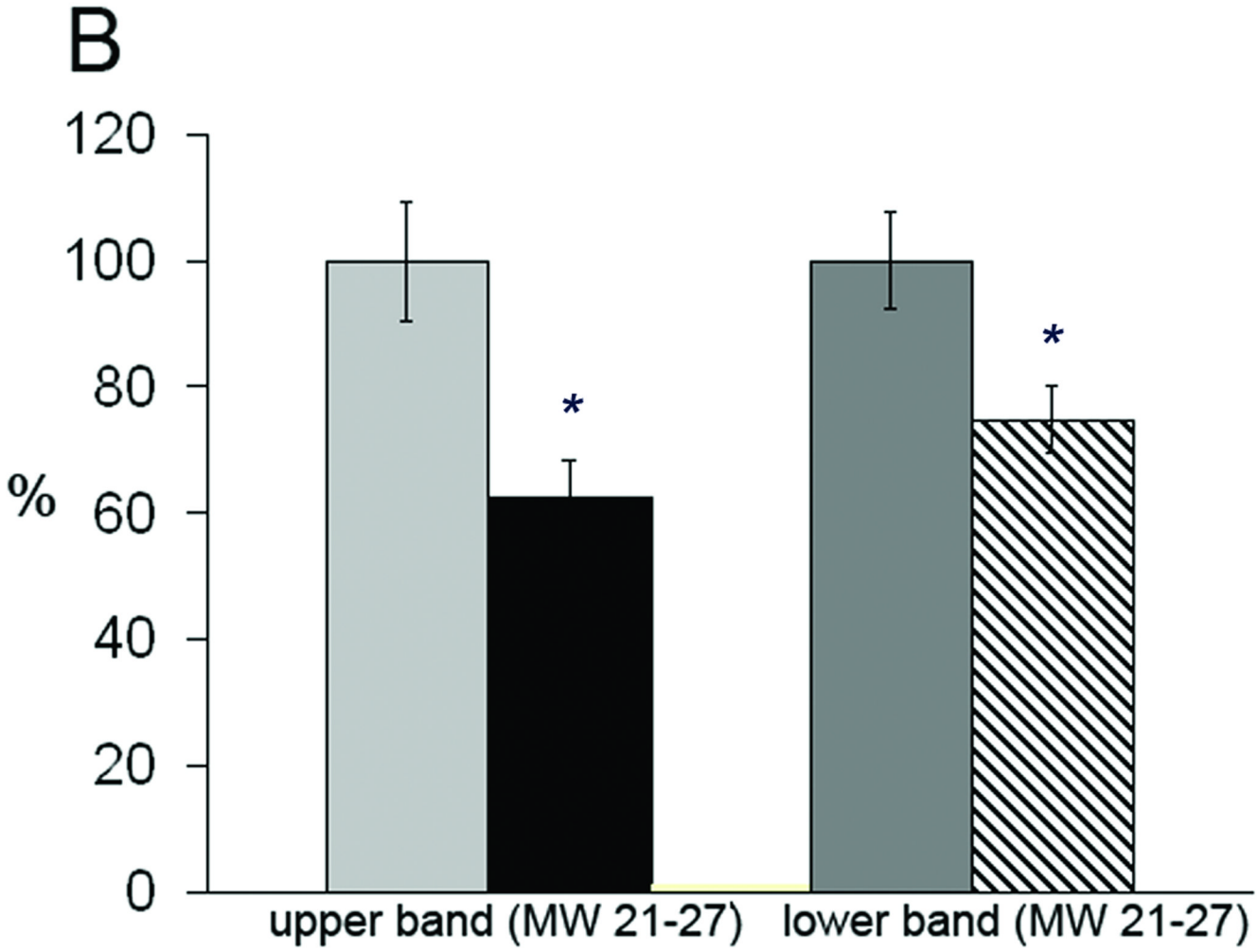

Figure 4.

Decreased lin7 protein in R6/2 mouse brain. (**A**) Graph showing the intensity of Lin7b staining in layer 5 pyramidal neurons of the motor cortex in R6/2 mice vs. wild type (WT) mice. There is an average reduction of 12% in the R6/2 mice. (**B**) Lin7b immunostaining in layer 5 motor cortex pyramidal neurons (arrows) in WT and R6/2 mice. (**C**) Graph showing the intensity of Lin7b staining in fiber tracts in striatum of WT and R6/2 mice, with an average reduction of 17% in the R6/2 mice. (**D**) Lin7b immunostaining in striata of WT and R6/2 mice. Asterisks indicate significant differences ($p < 0.05$) by Student *t*-test (**A, C**). Photomicrograph magnification = 20×; bar = 100 μm (**B, D**).

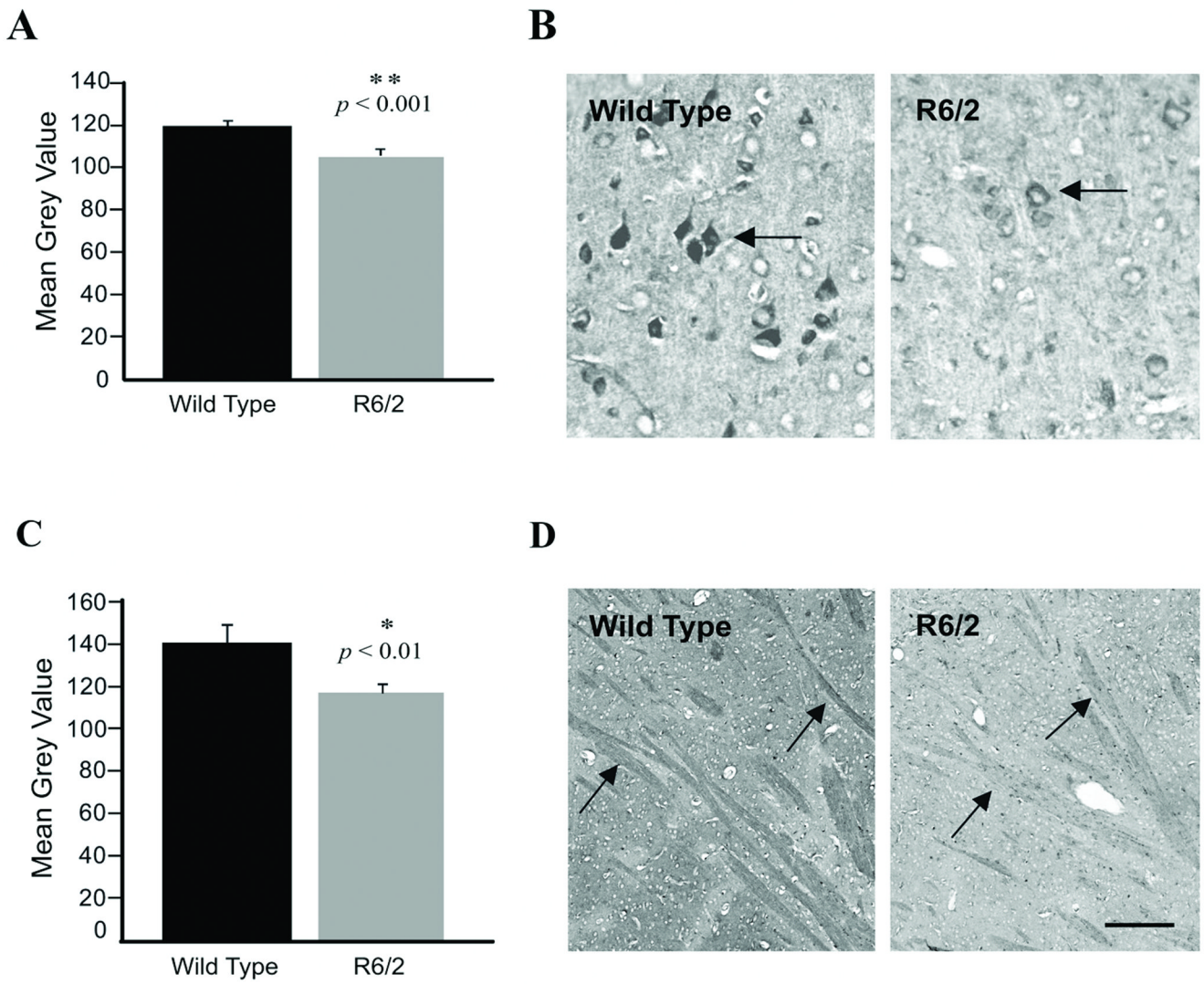

Figure 5.

Lin7b protein is decreased in Huntington disease (HD) brain. (**A**) Graph showing the intensity of Lin7b staining in somata and neuropil of layer 5 in BA4 (primary motor cortex) in 3 HD cases vs. 4 controls. There is a non-significant trend in average reduction of 53% in the HD cases ($p < 0.07$). (**B**) Graph showing Lin7b staining intensity in the BA4 layer 5 pyramidal neuron somata in 3 HD cases vs. 4 controls. There is an average reduction of 20% in the HD cases. *$p < 0.05$. by Student *t*-test. (**C**) Low- and high-magnification images of Lin7b immunostaining in control and HD BA4 cortex (left) bar = 500 μm, and BA4 layer 5 pyramidal neurons (right), bar = 40 μm.

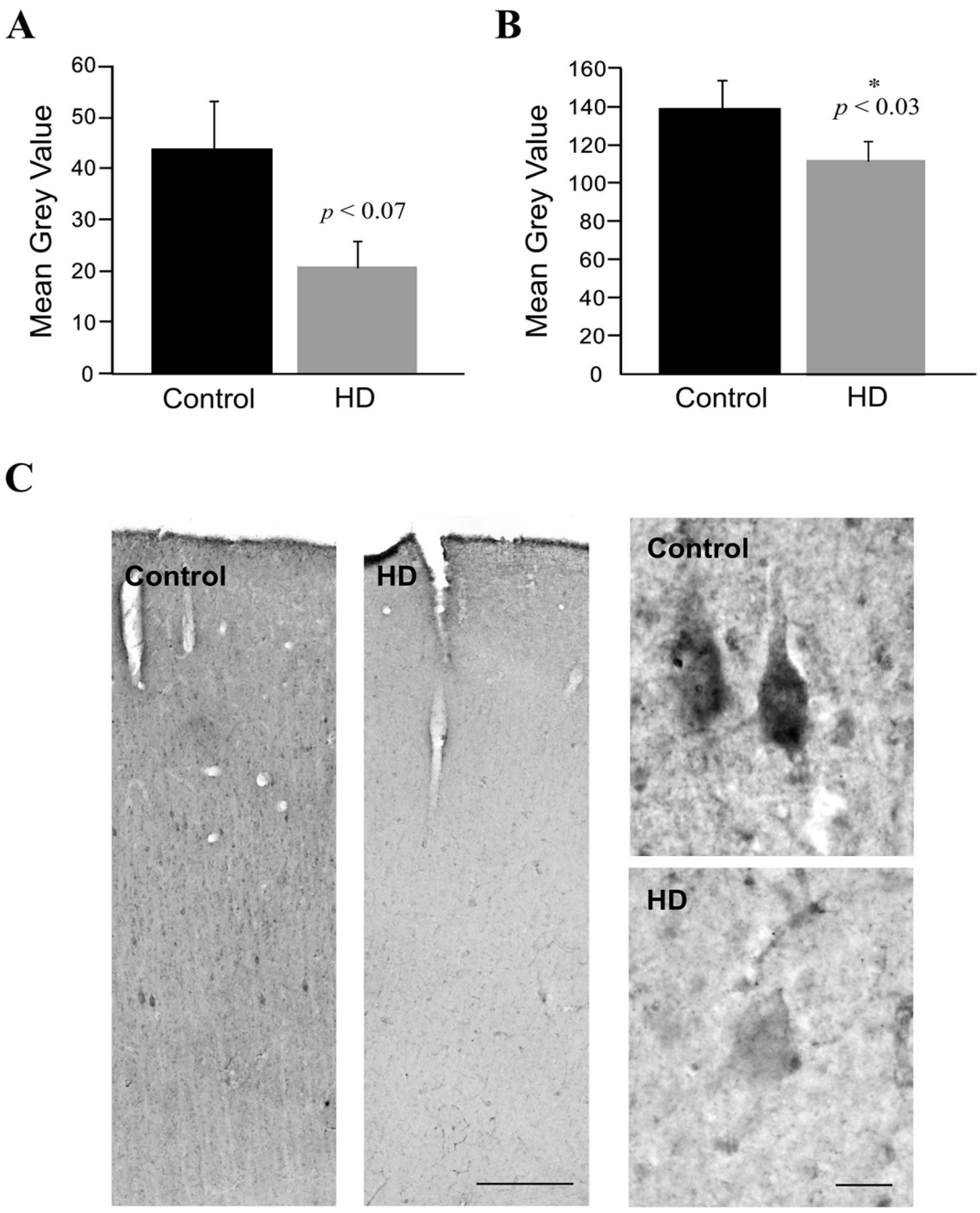

Figure 6.

Time course of Lin7 RNA changes in R6/2 mice. Lin7b RNA levels are significantly decreased in R6/2 mice at 6, 8, and 10 weeks of age (top panel). Lin7a RNA levels in R6/2 mice show a trend towards a decrease at 4 weeks of age and are significantly decreased at 6, 8, and 10 weeks of age (middle panel). Lin7c RNA levels are maintained in R6/2 mice at 4, 6, and 10 weeks of age, with a transient increase at 8 weeks (bottom panel). Quantitative PCR expression measures are presented as quotients of R6/2 vs. wild type (WT) values X 100 (% control) ± SEM (same scale). Samples comprised cortical RNA extracts from 4 WT and 4 R6/2 mice at 4 weeks, 12 WT and 12 R6/2 mice at 6 weeks, 8 WT and 8 R6/2 mice at

8 weeks, 7 WT and 7 R6/2 mice at 10 weeks. Asterisks represent statistical significance of $p < 0.05$ by 2-tailed Student *t* test.

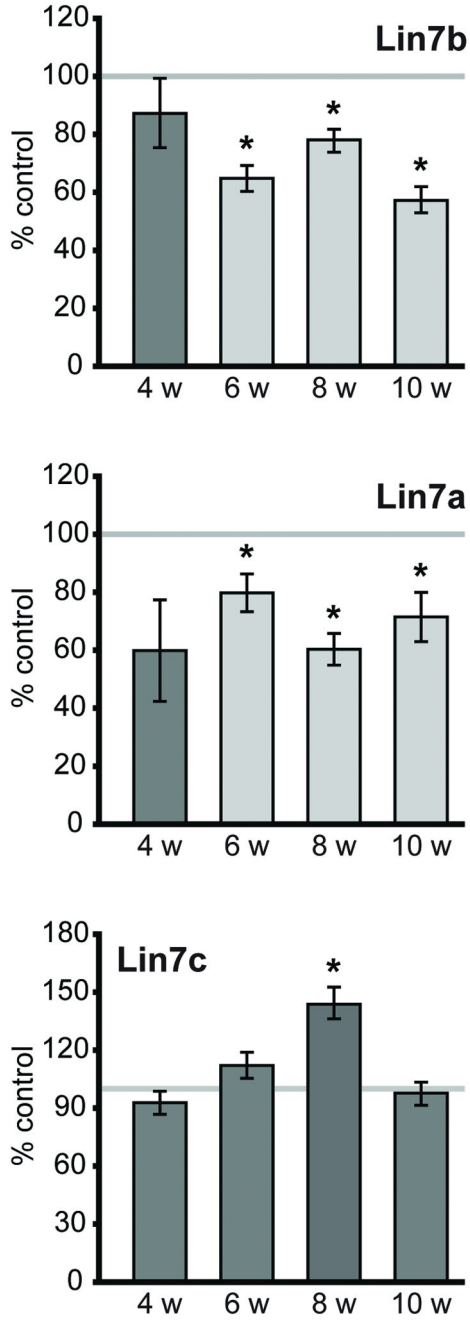

Figure 7.

Table 1

Human Brains used for Quantitative PCR and Immunohistochemistry

cortical region	number of cases	diagnosis	average age +/− SEM	age range	average CAG repeat length	CAG repeat length
New York Brain Bank						
BA4	8	control	61.5 +/− 4.0	44–82	n.a.	n.a.
	8	HD2, one HD3	68.6 +/− 4.1	54–80	42	40–45
BA9	7	control	60.3 +/− 4.3	44–82	n.a.	n.a.
	9	HD2, two HD3	67.1 +/− 4.1	54–80	42	40–45
New Zealand Brain Bank						
BA4	4	control	62.3 +/− 1.5	59–66	n.a.	n.a.
	4	HD2, one HD1, one HD3	63.0 +/− 2.6	56–68	42	41–43

Brains for the mRNA studies were obtained from the New York Brain Bank, Columbia University. BA4 and BA9 were taken from the same brains, except for 1 Huntington disease (HD) case and 1 control. Brains for the immunohistochemical studies were provided by the New Zealand Brain Bank, University of Auckland. HD Grade was determined according to Vonsattel (26).

Table 2

Selected mRNA Enrichments in Layer 5 Motor Cortex Neurons from Wild Type Mice

Probe set	gene symbol	Log2 FC	raw p-value	adjusted p value	Gene
1423756_s_at	Igfbp4	2.75	2.58E-05	1.91E-03	insulin-like growth factor binding protein 4
1431057_a_at	Prss23	2.62	2.72E-05	1.98E-03	protease, serine, 23
1440108_at	Foxp2	2.45	3.88E-04	9.27E-03	forkhead box P2
1449314_at	Zfpm2	2.07	1.37E-06	4.95E-04	zinc finger protein, multitype 2
1420150_at	Spsb1	1.96	2.35E-06	6.06E-04	splA/ryanodine receptor domain and SOCS box containing 1
1418047_at	Neurod6	1.92	2.98E-03	3.39E-02	neurogenic differentiation 6
1437067_at	Phtf2	1.83	1.68E-07	2.09E-04	putative homeodomain transcription factor 2
1452380_at	Epha7	1.82	2.95E-04	7.87E-03	Eph receptor A7
1422768_at	Syncrip	1.81	5.44E-06	8.75E-04	synaptotagmin binding, cytoplasmic RNA interacting protein
1416711_at	Tbr1	1.80	6.96E-06	9.54E-04	T-box brain gene 1
1427042_at	Mal2	1.80	6.44E-06	9.27E-04	mal, T-cell differentiation protein 2
1427017_at	Satb2	1.75	1.21E-04	4.56E-03	special AT-rich sequence binding protein 2
1428142_at	Etv5	1.74	1.92E-04	6.04E-03	ets variant gene 5
1460213_at	Golga4	1.71	1.37E-06	4.95E-04	Golgi autoantigen, golgin subfamily a, 4
1421882_a_at	Elavl2	1.69	2.47E-	6.23E-04	ELAV (embryonic lethal, abnormal vision, Drosophila)-like 2 (Hu antigen B)
1437422_at	Sema5a	1.67	061.64E-05	1.47E-03	sema domain, seven thrombospondin repeats (type 1 and type 1-like), transmembrane domain (TM) and short cytoplasmic domain, (semaphorin) 5A
1427481_a_at	Atp1a3	1.65	2.02E-05	1.47E-03	ATPase, Na+/K+ transporting, alpha 3polypeptide
1429434_at	Pik3ca	1.57	3.29E-03	3.64E-02	phosphatidylinositol 3-kinase, catalytic, alpha polypeptide
1455029_at	Kif21a	1.56	1.99E-04	6.18E-03	kinesin family member 21A
1452969_at	Atp2b1	1.54	2.02E-07	2.16E-04	ATPase, Ca++ transporting, plasma membrane1
1452205_x_at	Tcrb-V13	1.54	4.56E-06	7.93E-04	T-cell receptor beta, variable 13
1437147_at	Gabrg2	1.47	3.91E-05	2.40E-03	gamma-aminobutyric acid (GABA-A) receptor, subunit gamma 2
1449563_at	Cntn1	1.45	1.16E-06	4.89E-04	contactin 1
1434039_at	Appbp2	1.44	1.90E-04	6.02E-03	amyloid beta precursor protein (cytoplasmic tail) binding protein 2
1418637_at	Etv3	1.43	5.98E-06	8.98E-04	ets variant gene 3
1434298_at	Zfhx1b	1.34	4.31E-06	7.70E-04	zinc finger homeobox 1b

Probe set	gene symbol	Log2 FC	raw p-value	adjusted p value	Gene
1428248_at	Nfx1	1.14	2.20E-05	1.75E-03	nuclear transcription factor, X-box binding 1
1427231_at	Robo1	1.11	9.83E-04	1.67E-02	roundabout homolog 1 (Drosophila)
1434149_at	Tcf4	1.10	8.75E-05	3.80E-03	transcription factor 4
1452423_at	Pclo	1.09	5.37E-04	1.14E-02	piccolo (presynaptic cytomatrix protein)
1423322_at	Lin7c	1.09	9.97E-04	1.68E-02	lin 7 homolog c (C. elegans)
1428741_at	Elavl4	1.08	4.38E-05	2.55E-03	ELAV (embryonic lethal, abnormal vision, Drosophila)-like 4 (Hu antigen D)
1426582_at	Atf2	1.06	5.54E-06	8.80E-04	activating transcription factor 2
1458622_at	Ntrk2	1.05	1.53E-06	5.11E-04	neurotrophic tyrosine kinase, receptor, type 2
1448280_at	Syp	1.03	2.28E-06	6.00E-04	synaptophysin
1418817_at	Chmp1b	1.03	5.32E-04	1.14E-02	chromatin modifying protein 1B
1418683_at	Lin7b	0.49	4.75E-02	4.75E-02	lin 7 homolog b (C. elegans)

Differentially expressed probesets are presented as fold change of laser capture microdissection (LCM) neurons vs. whole cortex. P values were corrected for multiple testing using the False Discovery Rate (FDR) method (cutoff FDR $p < 0.05$). RNAs with the largest magnitude increases in LCM neurons are shown (FC = fold change). Probe-sets for expressed sequence tags (ESTs) and genes without annotation are not shown. In cases where multiple probesets represent the same mRNA, the probeset reporting the largest magnitude of change is shown. Full analysis is in the supplementary data.

J Neuropathol Exp Neurol. Author manuscript; available in PMC 2012 June 15.

Table 3

Selected mRNA Decreases in Layer 5 Neurons Motor Cortex of R6/2 versus Wild Type Mice

probe set	gene symbol	log2 FC	raw p-value	adjusted p value	gene
1422580_at	Myl4	−2.77	4.03E-10	9.45E-07	myosin, light polypeptide 4
1457984_at	Crh	−2.74	2.76E-10	9.16E-07	corticotropin releasing hormone
1452114_s_at	Igfbp5	−2.21	2.06E-10	8.44E-07	insulin-like growth factor binding protein 5
1438211_s_at	Dbp	−2.16	4.96E-10	9.71E-07	D site albumin promoter binding protein
1437671_x_at	Prss23	−2.02	2.72E-09	3.38E-06	protease, serine, 23
1434008_at	Scn4b	−2.00	1.05E-10	5.25E-07	sodium channel, type IV, beta
1427868_x_at	Myh1	−1.97	2.79E-07	6.26E-05	myosin, heavy polypeptide 1, skeletal muscle, adult
1418687_at	Arc	−1.86	4.60E-08	1.92E-05	activity regulated cytoskeletal-associated protein
1449556_at	H2-T23	−1.85	3.18E-07	6.70E-05	histocompatibility 2, T region locus 23
1436127_at	Crhbp	−1.77	1.57E-07	4.19E-05	corticotropin releasing hormone binding protein
1452205_x_at	Tcrb-V13	−1.77	2.95E-11	3.61E-07	T-cell receptor beta, variable 13
1417954_at	Sst	−1.75	5.56E-09	5.32E-06	Somatostatin
1424037_at	Itpka	−1.62	2.73E-08	1.31E-05	inositol 1,4,5-trisphosphate 3-kinase A
1416029_at	Klf10	−1.58	3.88E-09	4.26E-06	Kruppel-like factor 10
1427038_at	Penk1	−1.58	1.86E-06	2.20E-04	preproenkephalin 1
1418174_at	Dbp	−1.57	3.82E-10	9.45E-07	D site albumin promoter binding protein
1455978_a_at	Matn2	−1.56	3.70E-09	4.19E-06	matrilin 2
1422609_at	Arpp19	−1.54	6.61E-12	2.97E-07	cAMP-regulated phosphoprotein 19
1424474_a_at	Camkk2	−1.48	4.20E-10	9.45E-07	calcium/calmodulin-dependent protein kinase kinase 2, beta
1427683_at	Egr2	−1.47	1.70E-08	9.36E-06	early growth response 2
1449961_at	Rph3a	−1.46	9.75E-08	3.16E-05	rabphilin 3A
1418744_s_at	tesc	−1.45	1.42E-10	6.41E-07	Tescalcin
1448830_at	Dusp1	−1.43	5.08E-07	9.53E-05	dual specificity phosphatase 1
1459847_x_at	Gfra2	−1.42	6.37E-09	5.82E-06	Glial cell line derived neurotrophic factor family receptor alpha 2 (Gfra2), mRNA
1422256_at	Sstr2	−1.42	3.09E-10	9.29E-07	somatostatin receptor 2
1436275_at	Kcnip2	−1.39	1.14E-07	3.33E-05	KCHIP2A protein splice variant (KCHIP2 gene)
1423756_s_at	Igfbp4	−1.39	1.50E-08	8.78E-06	insulin-like growth factor binding protein 4
1419845_at	Dlx1	−1.34	1.05E-05	7.24E-04	Distal-less homeobox 1 (Dlx1), mRNA

probe set	gene symbol	log2 FC	raw p-value	adjusted p value	gene
1421477_at	Cplx2	−1.32	8.89E-07	1.34E-04	complexin 2
1448823_at	Cxcl12	−1.27	4.52E-08	1.92E-05	chemokine (C-X-C motif) ligand 12
1438934_x_at	Sema4a	−1.18	2.83E-07	6.26E-05	sema domain, immunoglobulin domain (Ig), transmembrane domain (TM) and short cytoplasmic domain, (semaphorin) 4A
1449980_a_at	Gabrd	−1.13	1.46E-08	8.78E-06	gamma-aminobutyric acid (GABA-A) receptor, subunit delta
1416561_at	Gad1	−1.10	4.55E-09	4.66E-06	glutamic acid decarboxylase 1
1436634_at	Robo3	−1.09	2.71E-07	6.16E-05	roundabout homolog 3 (Drosophila)
1416953_at	Ctgf	−1.03	1.04E-08	7.77E-06	connective tissue growth factor
1439239_at	Lin7b	−0.99	5.74E-06	4.89E-04	Lin 7 homolog b (C. elegans), mRNA
1455785_at	Kcna1	−0.99	3.43E-07	7.09E-05	Potassium voltage-gated channel, shaker-related subfamily, member 1 (Kcna1), mRNA
1421863_at	Vamp1	−0.90	2.26E-07	5.44E-05	vesicle-associated membrane protein 1
1417312_at	Dkk3	−0.83	1.00E-07	3.18E-05	dickkopf homolog 3 (Xenopus laevis)
1450350_a_at	jdp2	−0.83	4.78E-07	9.09E-05	Jun dimerization protein 2
1416505_at	Nr4a1	−0.80	1.15E-04	3.70E-03	nuclear receptor subfamily 4, group A, member 1

P values were corrected for multiple testing using the False Discovery Rate (FDR) method. Data are presented for a subset of probesets meeting criteria of log2 FC < −0.75 and FDR p < 0.05. The full analysis is available in supplementary data.

Table 4

Selected mRNA Increases in Layer 5 Motor Cortex Neurons of R6/2 versus Wildtype Mice

probe set	gene symbol	log2 FC	raw p-value	adjusted p-value	gene
1417457_at	Cks2	2.13	4.01E-11	3.61E-07	CDC28 protein kinase regulatory subunit 2
1438130_at	Taf15	1.76	1.44E-07	4.02E-05	TAF15 RNA polymerase II, TATA box binding protein (TBP)-associated factor
1430127_a_at	Ccnd2	1.57	4.68E-10	9.71E-07	cyclin D2
1456292_a_at	Vim	1.56	1.33E-09	1.94E-06	Vimentin
1418733_at	Twist1	1.27	5.50E-06	4.73E-04	twist gene homolog 1 (Drosophila)
1455039_a_at	Sin3b	1.21	2.00E-09	2.65E-06	transcriptional regulator, SIN3B (yeast)
1447669_s_at	Gng4	1.16	6.25E-09	5.82E-06	guanine nucleotide binding protein (G protein), gamma 4 subunit
1452959_a_at	Capn10	1.15	3.04E-07	6.52E-05	calpain 10
1416698_a_at	Cks1b	1.08	1.86E-06	2.20E-04	CDC28 protein kinase 1b
1434637_x_at	Sin3b	1.05	7.15E-09	6.31E-06	transcriptional regulator, SIN3B (yeast)
1417056_at	Psme1	1.04	1.31E-07	3.72E-05	proteasome (prosome, macropain) 28 subunit, alpha
1417185_at	Ly6a	1.03	6.11E-04	1.14E-02	lymphocyte antigen 6 complex, locus A
1442263_at	Rgs13	1.03	1.69E-05	1.01E-03	regulator of G-protein signaling 13
1424355_a_at	Sin3b	0.96	3.66E-08	1.67E-05	transcriptional regulator, SIN3B (yeast)
1419879_s_at	Trim25	0.94	3.83E-05	1.72E-03	tripartite motif protein 25
1448236_at	Rdx	0.91	6.99E-08	2.50E-05	Radixin
1428209_at	Bex4	0.91	1.72E-06	2.12E-04	brain expressed X-linked 4
1444908_at	Habp4	0.89	3.60E-05	1.66E-03	hyaluronic acid binding protein 4
1422649_at	Cntn6	0.87	2.76E-05	1.38E-03	contactin 6
1426412_at	Neurod1	0.87	5.43E-06	4.69E-04	neurogenic differentiation 1
1422457_s_at	Sumo3	0.87	2.44E-06	2.66E-04	SMT3 suppressor of mif two 3 homolog 3 (yeast)
1421840_at	Abca1	0.87	1.27E-06	1.70E-04	ATP-binding cassette, sub-family A (ABC1), member 1
1450783_at	Ifit1	0.87	1.86E-04	5.11E-03	interferon-induced protein with tetratricopeptide repeats 1
1439078_at	Klhl4	0.87	1.78E-05	1.05E-03	kelch-like 4 (Drosophila)
1455940_x_at	Wdr6	0.87	2.83E-07	6.26E-05	WD repeat domain 6
1417327_at	Cav2	0.86	1.93E-05	1.10E-03	caveolin 2
1428210_s_at	Chuk	0.86	2.70E-06	2.86E-04	conserved helix-loop-helix ubiquitous kinase
1436689_a_at	Aldh9a1	0.85	3.01E-07	6.48E-05	aldehyde dehydrogenase 9, subfamily A1

probe set	gene symbol	log2 FC	raw p-value	adjusted p-value	gene
1416371_at	Apod	0.84	4.09E-06	3.80E-04	apolipoprotein D
1448963_at	Nfyc	0.84	1.58E-08	9.11E-06	nuclear transcription factor-Y gamma
1435645_at	Mmd	0.84	9.18E-08	3.06E-05	monocyte to macrophage differentiation-associated
1448591_at	Ctss	0.84	1.55E-05	9.50E-04	cathepsin S
1443922_at	Rcor3	0.83	4.44E-04	9.20E-03	REST corepressor 3 (Rcor3), mRNA
1448595_a_at	Rex3	0.83	6.48E-06	5.35E-04	reduced expression 3
1449799_s_at	Pkp2	0.81	3.02E-06	3.11E-04	plakophilin 2
1435914_at	Ncor1	0.80	1.63E-04	4.66E-03	nuclear receptor co-repressor 1

P-values were corrected for multiple testing using the False Discovery Rate (FDR) method. Data presented are a subset of probesets meeting the criteria of FDR < 0.05 and log2FC > 0.8. The full analysis is available in the supplementary data.

Table 5

Comparison of mRNA Changes in R6/2 Layer 5 Motor Cortex Neurons to Human Huntington Disease Motor Cortex

mouse probe set	log2 FC	gene symbol	human probe set	log2 FC	gene symbol	gene
1416287_at	−0.93	Rgs4	204338_s_at	−1.29	RGS4	regulator of G-protein signalling 4
1417663_a_at	−0.50	Ndrg3	221082_s_at	−0.95	NDRG3	NDRG family member 3
1424474_a_at	−1.48	Camkk2	210787_s_at	−0.94	CAMKK2	calcium/calmodulin-dependent protein kinase kinase 2, beta
1416561_at	−1.10	Gad1	206670_s_at	−0.80	GAD1	glutamate decarboxylase 1 (brain, 67kDa)
1421863_at	−0.90	Vamp1	207101_at	−0.78	VAMP1	vesicle-associated membrane protein 1 (synaptobrevin 1)
1433888_at	−0.69	Atp2b2	211586_s_at	−0.77	ATP2B2	ATPase, Ca++ transporting, plasma membrane 2
1420955_at	−0.46	Vsnl1	203798_s_at	−0.77	VSNL1	visinin-like 1
1437147_at	−0.34	Gabrg2	206849_at	−0.76	GABRG2	gamma-aminobutyric acid (GABA) A receptor, gamma 2
1417954_at	−1.75	Sst	213921_at	−0.56	SST	somatostatin
1423362_at	−0.57	Sort1	212797_at	−0.76	SORT1	sortilin 1
1431191_a_at	−0.72	Syt1	203998_s_at	−0.69	SYT1	synaptotagmin I
1460203_at	−0.56	Itpr1	211323_s_at	−0.66	ITPR1	inositol 1,4,5-triphosphate receptor, type 1
1443724_at	−0.40	Jph3	220188_at	−0.66	JPH3	junctophilin 3
1450070_s_at	−0.50	Pak1	209615_s_at	−0.63	PAK1	p21/Cdc42/Rac1-activated kinase 1 (STE20 homolog, yeast)
1448690_at	−0.22	Kcnk1	204678_s_at	−0.62	KCNK1	potassium channel, subfamily K, member 1
1450646_at	−0.64	Cyp51	216607_s_at	−0.59	CYP51A1	cytochrome P450, family 51, subfamily A, polypeptide 1
1426499_at	−0.24	Sh3glb2	218813_s_at	−0.58	SH3GLB2	SH3-domain GRB2-like endophilin B2
1422609_at	−1.54	Arpp19	214553_s_at	−0.58	ARPP-19	cyclic AMP phosphoprotein, 19 kD
1434472_at	−0.28	Dusp3	201537_s_at	−0.57	DUSP3	dual specificity phosphatase 3 (vaccinia virus phosphatase VH1-related)
1449980_a_at	−1.13 -	Gabrd	208457_at	−0.57 -	GABRD	gamma-aminobutyric acid (GABA) A receptor, delta
1460214_at	0.70	Pcp4	205549_at	0.57	PCP4	Purkinje cell protein 4
1421255_a_at	−0.65	Cabp1	210181_s_at	−0.56	CABP1	calcium binding protein 1 (calbrain)
1457984_at	−2.74	Crh	205630_at	−0.51	CRH	corticotropin releasing hormone
1455672_s_at	−0.85	Cplx2	206368_at	−0.49	CPLX2	complexin 2

mouse probe set	log2 FC	gene symbol	human probe set	log2 FC	gene symbol	gene
1433716_x_at	−1.66	Gfra2	205722_s_at	−0.43	GFRA2	GDNF family receptor alpha 2
1416711_at	−0.66	Tbr1	220025_at	−0.42	TBR1	T-box, brain, 1
1434449_at	0.61	Aqp4	210068_s_at	0.99	AQP4	aquaporin 4
1450928_at	0.49	Id4	209291_at	0.98	ID4	inhibitor of DNA binding 4, dominant negative helix-loop-helix protein
1455556_at	0.48	Notch2	212377_s_at	0.78	NOTCH2	Notch homolog 2 (Drosophila)
1423754_at	1.20	Ifitm3	212203_x_at	0.70	IFITM3	interferon induced transmembrane protein 3 (1-8U)
1450644_at	0.42	Zfp36l1	211962_s_at	0.62	ZFP36L1	zinc finger protein 36, C3H type-like 1
1433761_at	0.64	Pde4dip	213388_at	0.60	PDE4DIP	phosphodiesterase 4D interacting protein (myomegalin)
1448666_s_at	0.41	Tob2	221496_s_at	0.60	TOB2	transducer of ERBB2, 2
1454725_at	0.68	G430041 M01Rik	213593_s_at	0.57	TRA2A	Transformer-2 alpha
1418640_at	0.61	Sirt1 Btg1	218878_s_at	0.50	SIRT1	sirtuin (silent mating type information regulation 2 homolog) 1 (S. cerevisiae)
1437455_a_at	0.42		200921_s_at	0.49	BTG1	B-cell translocation gene 1, anti-proliferative
1423824_at	0.41	Gpr177	221958_s_at	0.42	GPR177	G protein-coupled receptor 177
1438443_at	0.47	Zbtb20	205383_s_at	0.42	ZBTB20	zinc finger and BTB domain containing 20
1456003_a_at	0.59	Slc1a4	212810_s_at	0.40	SLC1A4	solute carrier family 1 (glutamate/neutral amino acid transporter), member 4

Comparison of mRNA changes in layer 5 samples from R6/2 vs. human Huntington Disease BA4 cortex homogenates. Gene expression changes common to both data sets were selected using a false discovery rate adjusted p value < 0.05 and an absolute log2FC cutoff of 0.4. Probe-sets for mRNAs chosen from among those showing the highest magnitude changes; decreases are above the horizontal bar; increases are below the horizontal bar. The complete list of common mRNA changes is available in the supplementary data.